THE ASTROPHYSICAL JOURNAL, 418:60–71, 1993 November 20

POLARIZED SCATTERING IN THE VICINITY OF GALAXIES

BRIAN W. MURPHY AND DAVID F. CHERNOFF[1]
Center for Radiophysics and Space Research, Cornell University, Ithaca, NY 14853
Received 1992 December 4; accepted 1993 May 28

ABSTRACT

Some bright cD galaxies in cluster cooling flows have Thomson optical depths exceeding 10^{-2}. A few percent of their luminosity is scattered and appears as diffuse polarized emission. We calculate the scattering process for different geometric combinations of luminosity sources and scattering media. We apply our results to galaxies, with and without active nuclei, immersed in cooling flows. We model observations of NGC 1275 and M87 (without active nuclei) in the presence of sky and galactic background fluxes which hinder the measurement of the scattered light at optical wavelengths. Current instruments are unable to detect the scattered light from such objects. However, when a galaxy has an active nucleus of roughly the same luminosity as the remainder of the galaxy in the *V*-band, *both* the total and polarized scattered intensity should be observable on large scales (5–30 kpc), meaning intensity levels greater than 1% of the background level. For typical active galactic nuclei and galaxy spectral distributions, the scattering is most easily detected at short (*U*) wavelengths. We point out that a number of such cases will occur. We show that the radiation pattern from the central nuclear region can be mapped using the scattering. We also show that the scattered light can be used to measure inhomogeneities in the cooling flow.

Subject headings: cooling flows — galaxies: clustering — polarization — radiative transfer — X-rays: galaxies

1. INTRODUCTION

A variety of observations suggest that large quantities of plasma and dark matter form halos around galaxies. Continuum X-ray brightness profiles (Jones & Forman 1984) demonstrate the existence of hot, distributed gas, while X-ray line emission (Stewart et al. 1984a) and centrally peaked X-ray images (Canizares, Stewart, & Fabian 1983) show that cooling of the gas occurs near the center of some galaxies (see Fabian, Nulsen, & Canizares 1991 for a review of cooling flows). Optical observations of rich clusters show substantial line emission emanating from filaments of gas in the cluster core and/or from the central dominant galaxy (Kent & Sargent 1979; Heckman 1981; Cowie et al. 1983). Deprojection and modeling of the X-ray data (Stewart et al. 1984 and others; a review is presented by Sarazin 1986) yield density profiles, mass inflow rates, and temperature distributions. Some of the mass accretion rates are enormous, e.g., 1000 $M_\odot$ yr^{-1} for the cooling flow of PKS 0745 − 191 (Fabian et al. 1985).

The inferred electron distribution implies Thomson optical depths of 10^{-3} to 10^{-2} over characteristic length scales (impact parameters) ranging from a galaxy radius of $\sim$20 kpc (or inner edge of a cooling flow) up to a cluster core radius of $\sim$100 kpc (or outer edge of a cooling flow). The scattered luminosity of the galaxy is roughly 0.1%–1% of its total luminosity and may be observable in some circumstances (Syunyaev 1982; Gil'fanov, Syunyaev, & Churazov 1987). Some galaxies with cooling flows have active nuclei e.g., for a selected sample of eight radio-loud quasars, Crawford & Fabian (1989) find that all eight reside in clusters surrounded by hot ionized gas. Study of the underlying light distributions from radio-loud quasars also indicates that many are giant elliptical galaxies (Hutchings, Crampton, & Campbell 1984) for which cooling flows are expected. In general, massive galaxies with active nuclei are prime prospects for observing scattered light, as suggested by Fabian (1989). He pointed out that a dense cooling flow around a quasar might yield an anisotropic optical continuum by the following mechanism. If the optical emission of the quasar is beamed and collinear with its radio emission, then it scatters in the hot plasma of the cooling flow and produces continuum emission aligned with the radio axis, as has been observed (Djorgovski et al. 1987; Chambers, Miley, & van Breugel 1987; McNamara & O'Connell 1993). Strong, frequency-independent polarization of the scattered radiation is the characteristic signature of the process. In a study of six high-redshift galaxies di Serego Alighieri, Cimatti, & Fosbury (1992) found that four show a high degree of linear polarization. Because the alignment of this polarization was perpendicular to the radio/optical axis, they concluded that the polarization is caused by light, from an anisotropic active nucleus, scattered into the line of sight by gas surrounding the galaxy.

For general wavelengths, Wise & Sarazin (1990) conclude that scattering is most likely detectable in the radio. If the scattering is measurable, Wise & Sarazin (1990) show that it can be used as a cosmological distance indicator as well as a probe of the physical conditions of the cooling flow. Recently, Wise & Sarazin (1992) examined the effects of inhomogeneities in cooling flows and temporal variations in the luminosity of the central source. The scattered radiation can provide a record of the luminosity over the last 10^5 yr and may help identify the parent population of high-luminosity active galactic nuclei (AGNs).

The drawback with observing scattering at radio wavelengths is that Faraday rotation effectively erases the polarization. Distinguishing the scattered light from other diffuse emission processes may be problematic once the polarization, the characteristic signature of the scattering process, is lost. At optical wavelengths Faraday rotation should be much less of a problem, but detection may be more difficult. In this paper we

[1] Presidential Young Investigator.

investigate the intensity and polarization properties of *visible* light scattered by the typical, inferred electron column densities. In our model a bright galaxy (with or without an active nucleus) is surrounded by a halo of ionized matter, either a cooling flow or hot gas confined by a cluster potential. We calculate the intensity of the scattered emission, the polarization fraction, and the two-dimensional pattern of polarization seen on the sky. While some polarized light is always produced in these situations, we discuss the observational difficulties associated with its detection. *We conclude that scattered, polarized light at optical frequencies should be detectable on large scales (5–30 kpc) in galaxies with sufficiently luminous nuclei and sufficiently dense cooling flows. The rough criteria are that the apparent luminosity of the nucleus exceed that of the parent galaxy and that the Thomson optical depth be of order 1%.*

Observation of scattered light probes (1) the angular distribution of the radiation from the nucleus and (2) the angular and radial distribution of material that surrounds the illuminating source. The first issue is especially relevant to theories that attempt to unify disparate classes of active galaxies with geometric beaming arguments (Barthel 1989). The second issue is important because the scattered polarized light can be used to probe length scales in cooling flows that have hitherto been inaccessible. X-ray observations have been the traditional tool for studying cooling flows, and much of our knowledge of them comes from the spectral and angular distribution recorded by the *Einstein Observatory* and more recently by *ROSAT* (Sarazin, O'Connell, & McNamara 1992). Here we show that scattered light provides a complementary source of information at angular scales smaller than the resolution of X-ray telescopes.

The plan of the paper is as follows. In §§ 2.1–2.6 we review the physics of scattering. We lay out our assumptions and approximations and solve several simple, model problems. In § 3.1 we show that the finite size of the luminosity source limits the fractional polarization at small distances from the center of the source. In §§ 3.2–3.6 we carry out calculations for the prototypical sources M87 and NGC 1275, cD's with active nuclei, and an atypical source, PKS 0745−191, and discuss limitations imposed by diffuse emission from the parent galaxy and the sky background. Readers primarily interested in applications will want to scan § 2.1 and § 2.6 and then continue with § 3. In § 4 we summarize our work and future possibilities for research.

2. PHYSICS OF SCATTERING

2.1. *Formalism*

We begin by assuming that a point source emits completely unpolarized light. Later, we will consider sources of finite extent. The scattering is assumed to be solely due to nonrelativistic electrons. Although heavy elements will be present if the gas is not primordial, the characteristic temperatures of cooling flows are large enough that grains will not survive except in the regions where star formation has begun. We ignore a photon's typical frequency shift $\delta\nu/\nu \simeq (kT/m_e c^2)^{1/2} = 0.13T_8^{1/2}$, so that the radiative transfer is frequency independent. We also assume that the optical depth is everywhere small, so that single-photon scattering is a good approximation. Finally, we assume that the luminosity of the central source is constant in time.

The basic geometry is illustrated in Figure 1. Our discussion follows the standard treatment of Thomson scattering (e.g., Rybicki & Lightman 1979, pp. 62 and 90). Let the source be at the origin. Let the direction of the light emitted be $\hat{\boldsymbol{k}}$ and let the direction of the scattered light be $\hat{\boldsymbol{n}}$. The plane in which $\hat{\boldsymbol{k}}$ and $\hat{\boldsymbol{n}}$ lie is the plane determined by the position of the source, the scattering material, and the observer. We define the first polarization vector, $\hat{\boldsymbol{\epsilon}}_1$, as the direction perpendicular to $\hat{\boldsymbol{k}}$ in that plane (or $\hat{\boldsymbol{k}} \times [\hat{\boldsymbol{n}} \times \hat{\boldsymbol{k}}]$) and the second, $\hat{\boldsymbol{\epsilon}}_2$, as the direction perpendicular to $\hat{\boldsymbol{n}}$ and $\hat{\boldsymbol{k}}$ (or $\hat{\boldsymbol{k}} \times \hat{\boldsymbol{n}}$).

The differential Thomson cross section is

$$\frac{d\sigma_T}{d\Omega} = r_e^2(1 - [\hat{\boldsymbol{\epsilon}} \cdot \hat{\boldsymbol{n}}]^2) , \tag{1}$$

where r_e is the classical radius of the electron. The unpolarized light emitted by the source may be decomposed into two components of equal intensity along $\hat{\boldsymbol{\epsilon}}_1$ and $\hat{\boldsymbol{\epsilon}}_2$. The scattered light is polarized because $\hat{\boldsymbol{\epsilon}}_1 \cdot \hat{\boldsymbol{n}}$ is, in general, not equal to $\hat{\boldsymbol{\epsilon}}_2 \cdot \hat{\boldsymbol{n}} = 0$. Let θ be the angle between $\hat{\boldsymbol{k}}$ and $\hat{\boldsymbol{n}}$. The observed light, that is, the light scattered into the line of sight, is described by two polarization directions, each perpendicular to $\hat{\boldsymbol{n}}$. We refer to the components perpendicular and parallel to $\hat{\boldsymbol{k}}$ by $\perp$ and $\parallel$, respectively. The "emissivities" for each mode at position s are

$$j_\perp(s) = \left(\frac{F}{2}\right) r_e^2 n_e ,$$

$$j_\parallel(s) = \left(\frac{F}{2}\right) r_e^2 n_e \cos^2\theta , \tag{2}$$

where F is the flux from the source and n_e is the electron density.

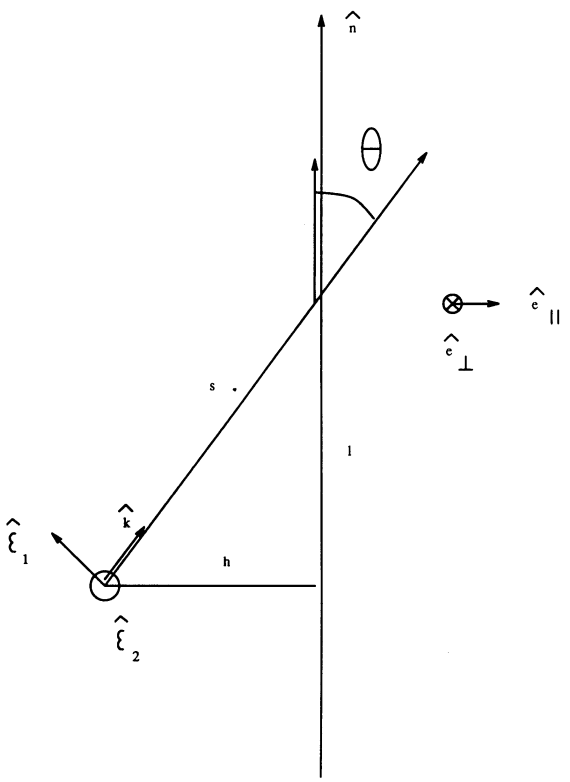

FIG. 1.—Photon leaves the source in the direction $\hat{\boldsymbol{k}}$, is scattered through an angle θ into the line-of-sight $\hat{\boldsymbol{n}}$. The polarization bases of the unscattered light, $\hat{\boldsymbol{\epsilon}}_1$ and $\hat{\boldsymbol{\epsilon}}_2$ (see § 2.1), and the scattered light, $\hat{\boldsymbol{e}}_\perp$ and $\hat{\boldsymbol{e}}_\parallel$, are illustrated.

The intensity seen by the observer is the integral over the line of sight (l) of the scattered emission in each polarization mode. The two polarization directions are defined by

$$\hat{e}_\perp = \hat{\epsilon}_1 \times \hat{n} ,$$
$$\hat{e}_\parallel = \hat{e}_\perp \times \hat{n} . \quad (3)$$

(In the quadrupole tensor, the signs of $\hat{e}_\perp$ and $\hat{e}_\parallel$ are irrelevant.) Figure 2 illustrates the polarization directions as viewed by the observer. They lie along the "tangential" ($\hat{e}_\perp$) and "radial" ($\hat{e}_\parallel$) directions of a circle whose center coincides with the luminosity source. They are the same at each point along a fixed line of sight. The intensities are

$$I_\perp = \int_{-\infty}^{\infty} j_\perp(s)dl = \frac{3L\sigma_T}{64\pi^2}\int_{-\infty}^{\infty}\frac{n_e(s)}{s^2}\,dl ,$$
$$I_\parallel = \int_{-\infty}^{\infty} j_\parallel(s)dl = \frac{3L\sigma_T}{64\pi^2}\int_{-\infty}^{\infty}\frac{n_e(s)l^2}{s^4}\,dl , \quad (4)$$

where L is the luminosity of the source. The fraction of polarized light is

$$\Pi = \left|\frac{I_\perp - I_\parallel}{I_\perp + I_\parallel}\right| . \quad (5)$$

For a single source the observed plane of polarization lies along $\hat{e}_\perp$.

2.2. *Point Source with Centered Power-Law Gas Distribution*

Now we consider a very simple scattering situation, a power-law electron distribution,

$$n_e(r) = n_c\left(\frac{r_c}{r}\right)^\alpha , \quad (6)$$

centered on the luminosity source. The total intensity of the scattered light at impact parameter h is

$$I = L\frac{n_c\sigma_T}{h}\left(\frac{r_c}{h}\right)^\alpha \frac{3(\alpha+3)\Gamma(\alpha+1)/2}{128\pi^{3/2}\Gamma(\alpha+4)/2} . \quad (7)$$

Here Γ is the Gamma function. The intensity of the scattered light is of course dependent on the flux of the source and the optical depth at the distance h. This expression for the total scattered intensity is identical to equation (2.2) of Wise & Sarazin (1992) modulo a difference in units of 4π. We see that

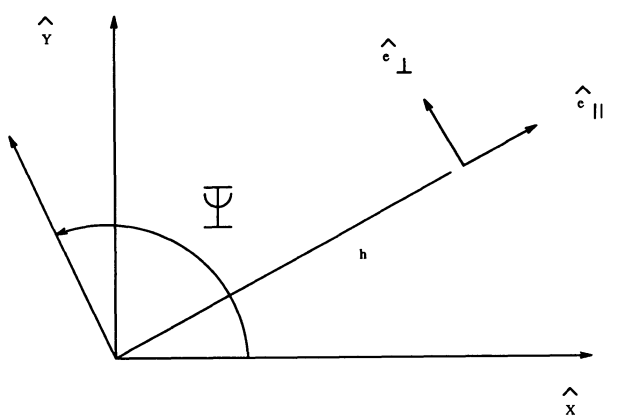

FIG. 2.—The parallel and perpendicular bases for the scattered light are displayed as seen by the observer.

$I \sim F(h)\tau(h)$, where $F(h) \sim$ flux and $\tau(h)$, is the optical depth $\sim(n_c\sigma_T h)(r_c/h)^\alpha$. The fraction of polarized light is

$$\Pi = \frac{\int_{-\pi/2}^{\pi/2}\cos^{2+\alpha}(\theta)d\theta}{\int_{-\pi/2}^{\pi/2}[1+\sin^2(\theta)]\cos^{2+\alpha}(\theta)d\theta} = \frac{1+\alpha}{3+\alpha} . \quad (8)$$

For a broad range of power laws a significant fraction of the scattered light is polarized.

The observer measures the Stokes parameters relative to some sky coordinate system ($\hat{x}$, $\hat{y}$) (see Fig. 2) of his choice. From our results above, the scattering from a point source is

$$I = I_\perp + I_\parallel ,$$
$$Q = (I_\perp - I_\parallel)\cos 2\Psi ,$$
$$U = (I_\perp - I_\parallel)\sin 2\Psi ,$$
$$V = 0 , \quad (9)$$

where Ψ is the angle between $\hat{x}$ and $\hat{e}_\perp$. For multiple sources of quasi-monochromatic radiation ($I_{\perp i}$, $I_{\parallel i}$, and Ψ_i), the Stokes parameters add up to give ($I_{\rm tot}$, $Q_{\rm tot}$, $U_{\rm tot}$, $V_{\rm tot}$). The total intensity seen at a point is $I_{\rm tot}$, the total polarization is

$$\Pi_{\rm tot} = \frac{\sqrt{Q_{\rm tot}^2 + U_{\rm tot}^2 + V_{\rm tot}^2}}{I_{\rm tot}} , \quad (10)$$

and the angle of polarization is given by

$$\tan 2\Psi = \frac{U_{\rm tot}}{Q_{\rm tot}} . \quad (11)$$

2.3. *Point Source with Off-Center Gas Distribution*

2.3.1. *Analytic Limiting Forms*

In general, the gas responsible for the scattering is hardly likely to be symmetrically distributed about the illuminating source. In this section we relax the assumption of symmetry. We illustrate how displacing the luminosity center from the gas center alters the polarization fraction, the intensity of the scattered light, and the geometry of the polarization pattern. Assume an electron distribution with a scale-free power-law profile (see eq. [6] with $\alpha = 1$) centered at the point $\boldsymbol{r}_0 = (x_0, y_0, z_0)$ and a luminosity point source at the origin. Without loss of generality, we assume that the observer views the scattered light along the $\hat{z}$ direction. We derive limiting forms for the scattering and polarization for lines of sight passing near $\boldsymbol{r}_0$ and the origin, where the scattered intensity has local maxima. Elsewhere, the paucity of electrons and/or the dilution of flux from the source decreases the scattered intensity. We provide a systematic expansion in angular harmonics that describes the asymptotic behavior far from the center.

Let the impact parameter of the line of sight with respect to the origin be $p = \sqrt{x^2 + y^2}$ and with respect to the density peak be $q = \sqrt{(x-x_0)^2 + (y-y_0)^2}$. Letting $I_0 = 3Ln_c\sigma_T r_c/64\pi^2$, equation (4) becomes

$$(I_\perp) = I_0\int_{-\infty}^{\infty} dl\,\frac{1}{(p^2+l^2)[q^2+(l-z_0)^2]^{1/2}} ,$$
$$(I_\parallel) = I_0\int_{-\infty}^{\infty} dl\left(\frac{l^2}{p^2+l^2}\right)\frac{1}{(p^2+l^2)[q^2+(l-z_0)^2]^{1/2}} , \quad (12)$$

First, for lines of sight that pass near the density peak ($q/z_0 \to 0$ and finite p/z_0), we expand in powers of (q/z_0) and integrate

term by term to find

$$I_\perp \to \frac{I_0}{(z_0^2+p^2)}\left\{-2\ln\left(\frac{q}{z_0}\right)+\ln 4\left[1+\left(\frac{p}{z_0}\right)^2\right] - \frac{2\tan^{-1}(p/z_0)}{(p/z_0)}+O\left(\frac{q}{z_0}\right)\right\},$$

$$I_\parallel \to \frac{I_0 z_0^2}{(z_0^2+p^2)^2}\left\{-2\ln\left(\frac{q}{z_0}\right)+\ln 4\left[1+\left(\frac{p}{z_0}\right)^2\right] + \left[\left(\frac{p}{z_0}\right)^2-1\right]\left[\frac{\tan^{-1}(p/z_0)}{(p/z_0)}+1\right]+O\left(\frac{q}{z_0}\right)\right\}. \quad (13)$$

Formally, $I_\perp$ and $I_\parallel$ diverge logarithmically near the density peak, although one (or both) of the assumptions, optically thin radiative transfer and unbounded growth in density near $\boldsymbol{r}_0$, must break down. As $q \to 0$ the fractional polarization approaches the limit:

$$\Pi \to \frac{p^2}{2z_0^2+p^2} \to \frac{r_0^2-z_0^2}{r_0^2+z_0^2}. \quad (14)$$

When the peak and luminosity source lie in the same plane ($p/z_0 \to \infty$), the fractional polarization is a maximum. At a fixed-impact parameter, a larger line-of-sight separation lowers Π. To summarize, *significant fractional polarization is expected near a density peak whose three-dimensional displacement from the luminosity source is less than a modest multiple of the impact parameter.*

A systematic expansion for scattering at large impact parameters may be developed as follows. We express the density field (centered at $\boldsymbol{r}_0$ with the form $1/|\boldsymbol{r}-\boldsymbol{r}_0|$) in spherical harmonics and powers of the distance from the origin. The integral over the line of sight is converted to an angular integral and carried out term by term. Let (r_0, θ_0, ϕ_0) be the spherical coordinates of the density field center, measured with respect to the origin (the luminosity point source). The impact parameter of the line of sight in the $\hat{z}$ direction is p at angle ϕ. For $p > r_0$ we have the exact solution:

$$\begin{pmatrix} I_\perp \\ I_\parallel \end{pmatrix} = I_0 \sum_{\substack{l=0\ldots\infty \\ |m|\le l \\ m+l\,\mathrm{even}}} \begin{pmatrix} A_{lm} \\ B_{lm} \end{pmatrix} e^{im(\phi-\phi_0)} P_l^m(\cos\theta_0)\frac{r_0^l}{p^{l+2}}, \quad (15)$$

where

$$A_{lm} = 2(-1)^{(m+l)/2}\frac{(l-m)!}{(2l+1)!!},$$

$$B_{lm} = \left[1-\frac{(l-m+2)(l+m+2)}{2(2l+3)}\right]A_{lm}. \quad (16)$$

To order $l=2$, these expansions yield the following explicit forms:

$$\frac{I_\perp}{I_0} = \frac{2}{p^2}+\frac{4r_0}{3p^3}\sin\theta_0\cos(\phi-\phi_0) + \frac{4r_0^2}{5p^4}\left\{\sin^2\theta_0\cos[2(\phi-\phi_0)]-\frac{1}{6}(3\cos^2\theta_0-1)\right\},$$

$$\frac{I_\parallel}{I_0} = \frac{2}{3p^2}+\frac{4r_0}{15p^3}\sin\theta_0\cos(\phi-\phi_0) + \frac{4r_0^2}{35p^4}\left\{\sin^2\theta_0\cos[2(\phi-\phi_0)]+\frac{1}{6}(3\cos^2\theta_0-1)\right\}. \quad (17)$$

The fractional polarization at large distances (to order $l=1$) is

$$\Pi \to \frac{1}{2}+\frac{r_0}{10p}\sin\theta_0\cos(\phi-\phi_0). \quad (18)$$

To summarize, *at large distances from the luminosity source and density peak, the scattering approaches the simple form for a point source with a centered power law* (see § 2.2). As $p \to \infty$, Π agrees with equation (8) for the adopted density power law ($\alpha = 1$).

The term by term integration may also be carried out for lines of sight that pass within the spherical shell of radius $p < r_0$, but in this case there are three separate regions of integration and the formulae are more complicated. A consistent expansion is most easily derived using cylindrical coordinates. To summarize the steps: we expand $1/|\boldsymbol{r}-\boldsymbol{r}_0|$ using modified Bessel functions (I_m and K_m), perform the line-of-sight integral in z, and then substitute a series expansion for I_m (8.445 of Gradshteyn & Ryzhik 1980; hereafter G&R) and an integral definition for K_m (G&R, 8.432.3). An asymptotic expansion of the integrand gives integrals which may be reduced term by term to Beta functions. The results can be compactly expressed using $s = \sqrt{(x^2+y^2)/(x_0^2+y_0^2)}$ and $t = \sqrt{z_0^2/(x_0^2+y_0^2)}$; we assume the ordering $s, t < 1$. This ordering means that (i) the line of sight passes much closer to the luminosity source than the density peak and (ii) the density peak's displacement along the line of sight is less than or equal to its projected separation (other orderings may also be analogously treated). Let

$$F_m(s,t,\delta) = \sum_{k=0}^{\infty}\left[\frac{s^{m+2k+1+\delta}}{k!(m+k)!}\right]\sum_{n=0}^{\infty}\frac{(-2)^n}{n!} \times \Gamma\left(m+k+\frac{n+1+\delta}{2}\right)\Gamma\left(k+\frac{n+1+\delta}{2}\right) \times [(s-it)^n+(s+it)^n], \quad (19)$$

and let $a_i = 1$ for $i > 0$ and $a_0 = \frac{1}{2}$:

$$I_\perp = \frac{I_0}{p^2}\sum_{m=0}^{\infty} a_m \cos m(\phi-\phi_0)F_m(s,t,0)$$

$$(I_\parallel) = \frac{I_0}{p^2}\sum_{m=0}^{\infty} a_m \cos m(\phi-\phi_0)\left[\frac{F_m(s,t,0)}{2}-F_m(s,t,1)\right]. \quad (20)$$

Using the above expressions it is straightforward to give $I_\parallel$ and $I_\perp$ to order $s^{\mu_s}t^{\mu_t}$ for $\mu_s+\mu_t < M$ for a given M. For $M=2$ the result is independent of t,

$$\frac{I_\perp}{I_0} = \frac{s\pi}{p^2}\left[1-\frac{2}{\pi}s+s\cos(\phi-\phi_0)\right], \quad (21)$$

and

$$\frac{I_\parallel}{I_0} = \frac{s\pi}{2p^2}\left[1-\frac{4}{\pi}s+s\cos(\phi-\phi_0)\right]. \quad (22)$$

The divergence in intensity as $p \to 0$ may be traced to the assumption of a luminous point source. Note that the limiting behavior of the fractional polarization is

$$\Pi \to \frac{1}{3}\left[1+\frac{8s}{3\pi}-2s\cos(\phi-\phi_0)\right], \quad (23)$$

which is the same as for a point source embedded in a scattering gas of uniform density. To summarize, *the fractional*

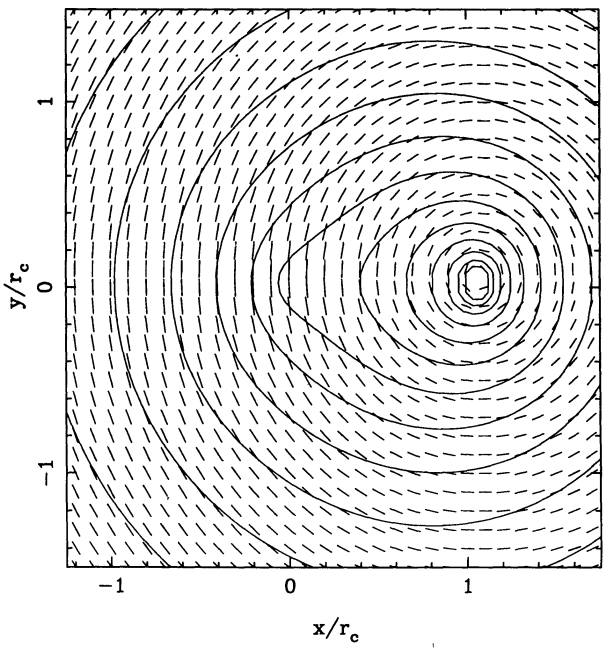

FIG. 3a

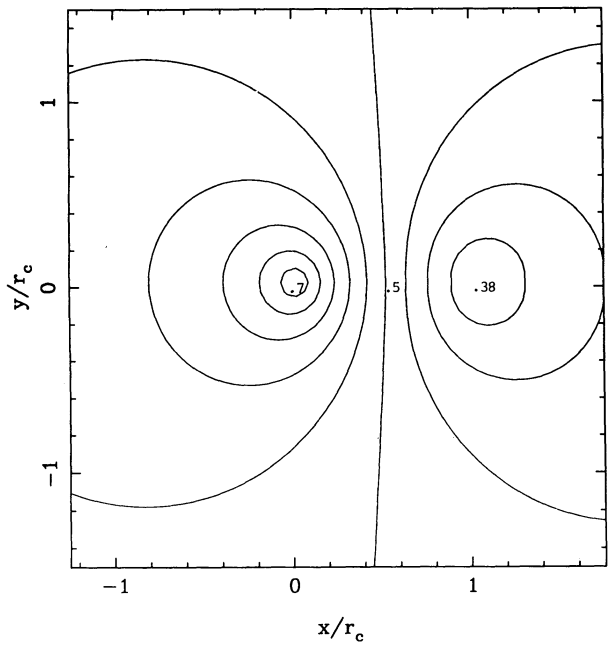

FIG. 3b

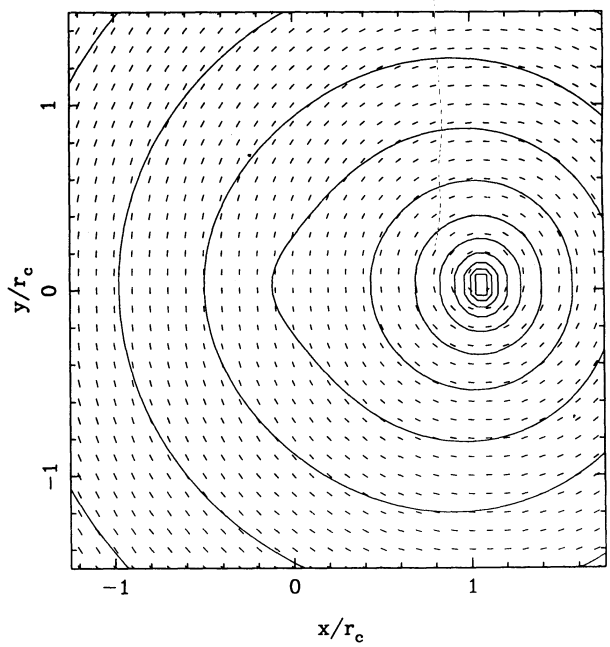

FIG. 3c

FIG. 3.—(*a*) Polarization fraction (length of the line segments), the angle of polarization (orientation of the line segments), and the intensity of the scattered light (contours) for a luminosity source coplanar with the gas center. Here the luminosity source is coplanar with and $1r_c$ to the right of the gas-density origin. The contour interval is 0.5 mag ($10^{0.2}$). (*b*) Contours of polarization fraction are shown for the same geometry as in Fig. 3*a*. The contour interval is 0.04. (*c*) Same as (*a*), but the luminosity source is $4r_c$ out of the plane of the gas-density origin.

polarization expected in the vicinity of a luminosity point source approaches that of a point source in a uniform density medium.

2.3.2. *Numerical Results*

We now proceed with a more detailed description via a numerical calculation. We have carried out the quadratures in equation (4) for a grid of 100 by 100 lines of sight. As in the analytic work above, we take a scale-free power law (eq. [6] with $\alpha = 1$) for the density distribution. The source is located in the plane of the gas center (coplanar geometry, $z_0 = 0$) or displaced out of the plane ($\sqrt{x_0^2 + y_0^2}/z_0 = 1/4$). Figure 3*a* shows the polarization fraction (length of the line segments), the angle of polarization (direction of the line segments), and the intensity of the scattered light (contours) for the coplanar geometry. Figure 3*a* and subsequent figures are centered about the gas-density maximum (r_0). The maximum intensity occurs near the source, while a local maximum occurs near the gas center. The numerically derived fractional polarization, shown in Figure 3*b*, is a minimum near the source (~ 0.35; compare eq. [23]) and a maximum near the gas center (~ 0.75; compare eq. [14]). In the vicinity of the gas center and the point source, the polarization ranges between these extremes; at large radii it approaches 0.5, as would be expected for a point source embedded in a gas following r^{-1} power law (eqs. [8] or [18]). Of course, at the gas center the numerically determined fractional polarization should approach its maximum value of unity, while at the source it should go to $\frac{1}{3}$. These limits are only approximately observed in our numerical model because of the finite resolution in the 100 × 100 grid. When the source and gas center are displaced out of the plane (Fig. 3*c*), scattering near the gas center is diminished (the flux from the source at the gas center is less; compare eq. [13]) and the polarization decreases (the scattering angle θ becomes small at the high-density region; compare eq. [14]).

2.4. *Comparison of Center and Off-Center Gas Distributions*

We now consider the scattering when both a centered and off-centered distribution are present. We want to derive simple criteria to distinguish which type of scattering dominates. Of course, since the radiative transfer is linear in our approximation, the individual results may be simply added to give I_{tot} and Π_{tot} as described in § 2.2. First, we assume that both distributions lie in the same plane and that the off-center distribution is a power law with $\alpha = 1$. The intensity from the

off-center "clump" is given by

$$I_{\perp}^{\rm cl} = \frac{I_0}{(1-u^2)^{1/2}p^2}\ln\left[\frac{1+\sqrt{1-u^2}}{1-\sqrt{1-u^2}}\right],$$

$$I_{\parallel}^{\rm cl} = \frac{I_0}{(1-u^2)^{3/2}p^2}\left[\sqrt{1-u^2} - \frac{u^2}{2}\ln\left(\frac{1+\sqrt{1-u^2}}{1-\sqrt{1-u^2}}\right)\right], \quad (24)$$

where $u = q/p$ and q, p, and I_0 have the same definitions as above. In the limit that the clump is centered on the galaxy, $u \to 1$ results in equations (7) and (8) are retrieved.

For comparison, the ratio of $I^{\rm cl} = I_{\perp}^{\rm cl} + I_{\parallel}^{\rm cl}$, the total scattered intensity from the off-center clump, to $I^{\rm gal}$, the intensity from an assumed galactic halo given by equation (7), at the same impact parameter, is

$$\frac{I^{\rm cl}}{I^{\rm gal}} = \frac{3f(u)}{8}\left(\frac{n_c^{\rm cl}r_c^{\rm cl}}{n_c^{\rm gal}r_c^{\rm gal}}\right), \quad (25)$$

where $f(u)$ is a function which diverges logarithmically at small u (this ignores the core radius of the clump). The quantities $n_c^{\rm gal}$, $n_c^{\rm cl}$, $r_c^{\rm gal}$, and $r_c^{\rm cl}$ are the scaling densities and radii used in equation (6) for the off-center clump and the galaxy's gas distribution at the center. For fixed column densities of the clump and galaxy, the ratio depends only upon $f(u)$. At a fixed distance from the clump center (e.g., its core radius), $u \to 0$ as the clump displacement from the galaxy center increases. The result suggests that the clump scattering dominates halo scattering at large galactic radii but is sensitive to the large extent assumed for the clump ($\alpha = 1$).

It is straightforward to evaluate $I^{\rm cl}/I^{\rm gal}$ for arbitrary power laws for galaxy ($\alpha^{\rm gal} \geq 0$) and clump ($\alpha^{\rm cl} \geq 2$) when the line-of-sight contribution to scattering is dominated by the points of closest approach. We find the intensity ratio scales as

$$\frac{I^{\rm cl}}{I^{\rm gal}} \approx \left(\frac{n_c^{\rm cl}r_c^{\rm cl}}{n_c^{\rm gal}r_c^{\rm gal}}\right)\left(\frac{p}{r_c^{\rm gal}}\right)^{\alpha^{\rm gal}-1}\left(\frac{r_c^{\rm cl}}{q}\right)^{\alpha^{\rm cl}-1}. \quad (26)$$

For the massive cD galaxies with which we are concerned, $\alpha^{\rm gal} \approx 1$. Thus, for a sufficiently concentrated clump profile ($\alpha^{\rm cl} \geq 2$), we see that at a fixed distance from the clump center, the ratio of column densities fixes the ratio of the brightnesses. To summarize, *our comparison shows that the most significant factor dictating the clump-to-halo brightness ratio is the column density ratio.* If the off-center clump has an extended ($\alpha = 1$) distribution, the brightness ratio increases slowly (logarithmically) as it is displaced from the luminosity center. For concentrated clumps, the ratio is insensitive to the displacement. We note that we have not taken into account the extended nature of the galaxy. Had we compared the scattered intensity of the off-center clump to the scattered intensity of an extended galaxy instead of a point source, then the ratio would have been larger (see § 3.1).

2.5. *Multiple-Point Luminosity Sources*

In this section we examine the polarization pattern produced by the combination of two point sources embedded in a scale-free power-law scattering distribution ($\alpha = 1$ in eq. [6]). For illustrative purposes, we take the two sources to be equal in luminosity and equidistant from the gas center as seen in projection. One source remains fixed in the plane of the sky that passes through the gas center, and the other source is placed at predetermined intervals perpendicular to this plane. In this example, the sources are oriented so that one lies at an angle of $\pi/2$ and the other at an angle of 0 with respect to the gas center.

The total polarization at any given point can be calculated numerically using equations (4), (9), and (10). First, the integrals in equations (4) are numerically evaluated for a grid of 100 × 100 lines of sight for a single source. Then, the contribution of a second source equivalent to the first but rotated by $\pi/2$ is calculated and combined pointwise on the grid. Figure 4*a* shows the fractional polarization, the angle of polarization, and the intensity of scattered light for a configuration with both point sources lying in the plane of the gas center. As expected, the intensity has local maxima at the sources and at the center of the scattering distribution. The new feature, however, is that there are two regions of destructive interference seen as lobes of low polarization. It is easy to understand their cause. Consider the right triangle defined by the line connecting the two sources and the angles $\pi/4$ at each source. Clearly, near the third vertex of the triangle, the polarization angle of one source is perpendicular to the other and the flux from the sources is identical, so the scattered polarized intensity is zero. On the other hand, the largest polarization must occur midway on the straight line connecting the two sources and, also, at large distances from both. In both of these regions the polarization adds constructively and approaches the asymptotic value of 50% for $\alpha = 1$. We conclude that multiple sources complicate the polarization pattern where the scattering intensities are roughly equivalent.

The remaining plot, Figure 4*b*, shows the polarization pattern when the source at $\pi/2$ (the "secondary source") is moved along the line of sight to a distance 4 times its projected distance from the gas center. As the source is moved out of the plane of the sky, the scattering properties undergo noticeable changes. (It does not matter, however, whether the source is moved into the foreground or the background; both directions will show the same change.) First, the intensity of the scattered light around the secondary source decreases from its maximum value in the plane (which is consistent with the previous example of a single source). Second, the fractional polarization in the vicinity of the secondary source drops in this example from roughly 35% to 20% as line-of-sight distance goes to its maximum value (which is also consistent with our previous example of a single source). Finally, the area of interference of the two sources (the two low-polarization lobes) approaches the secondary source as it moves out of the plane. The lobes occur where both galaxies provide the same flux, so that the parallel and perpendicular components of the light scattered by both sources negate one another. That projected location must be closer to the secondary source where it is moved out of the plane of the sky.

2.6. *Summary*

Our examples show that the geometry of the source and of the electron distribution governs the polarization patterns in a simply understood fashion. One can envision many potential applications. It may be possible to constrain the three-dimensional position of luminosity sources by studying such patterns. For example, consider a luminous galaxy located off center in a spherical-cluster potential that is filled with ionized gas. The offset position of the galaxy along the line of sight with respect to the cluster center can be determined if enough of the light scattered by the cluster gas can be detected and mapped. Another potential application is to use scattering measurements to locate, identify and map inhomogeneities,

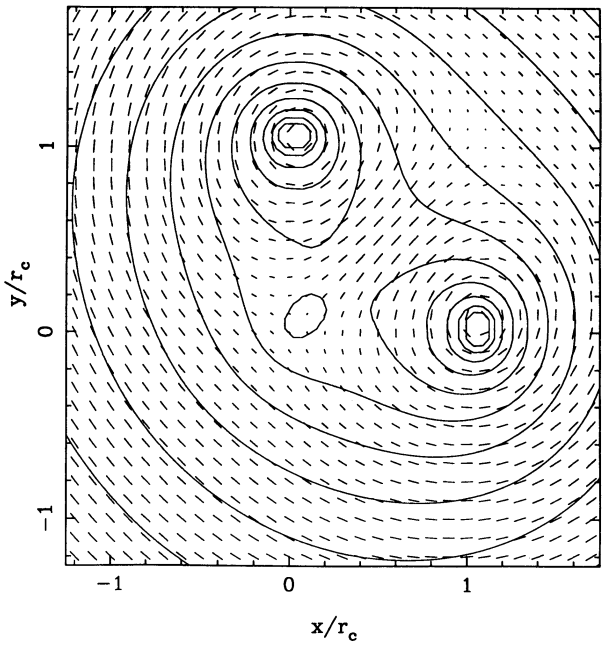

FIG. 4a

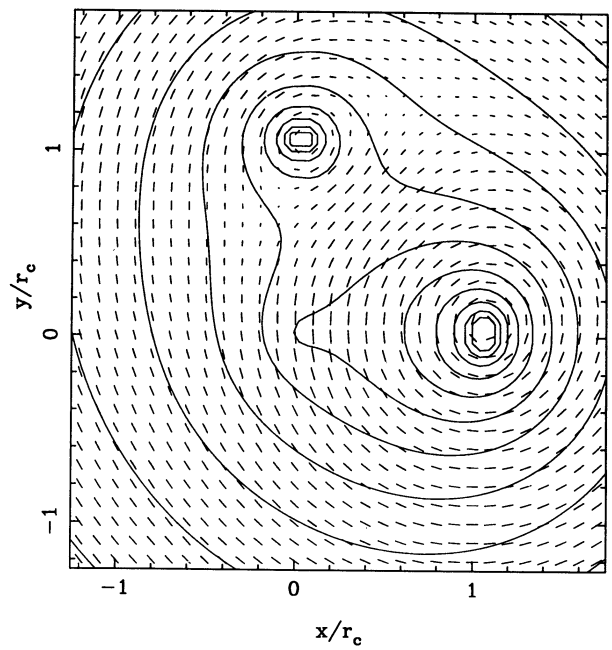

FIG. 4b

FIG. 4.—(*a*) Same as Fig. 3*a* but with two luminosity sources coplanar with the gas-density origin. (*b*) Same as Fig. 3*a* but with two luminosity sources, one coplanar with the gas-density origin and one $4r_c$ out of the plane.

e.g., as gas becomes thermally unstable in a cooling flow. Finally, in a cluster with many galaxies present, the constructive and destructive effects in the polarized scattering lead to complicated neighbor-neighbor interactions. Detailed polarization maps may be used to model the three-dimensional distribution of galaxies in a cluster. A prime candidate is the cluster 2A 0335+096 (Sarazin et al. 1992). This cluster has a central D galaxy with a bright companion nucleus at a radius of 6 kpc. Added to this are two other galaxies located at distances of 40 kpc. Throughout this region, *ROSAT* observations indicate that the gas density is slightly less than 0.1 cm^{-3}. In the section that follows we consider additional physical effects that complicate the use of polarization as a potential observational tool.

3. ESTIMATES OF SCATTERING FROM ACTUAL SOURCES

3.1. *Extended Luminosity Sources*

We have previously considered the intensity of the polarized scattering, the angle of polarization, and the fractional polarization produced by point-like luminosity sources. In practice, the spatial extent of the luminosity source may also be important, e.g., if galactic emission is scattered by gas within a few core radii of the galaxy itself. In this section we consider the continuum limit for the luminosity source and characterize the differences in the scattered emission for a point source and an extended source.

Let ρ_L be the luminosity density and n_e be the scattering density, each assumed to be spherically symmetric about the origin. Without loss of generality, choose the line of sight in the $\hat{z}$ direction and $p\hat{y}$ as the impact parameter. Let l be the distance along the line of sight and s the distance between (x, y, z) and $(0, p, l)$. The scattered intensity and polarized intensity are then given by integrals over the volume and along the line of sight:

$$[I] = \frac{3\sigma_T}{64\pi^2}\int dx\,dy\,dz\,dl\,\frac{\rho_L(x,y,z)n_e(l)}{s^4}[s^2 + (l-z)^2]\,,$$

$$[P] = \frac{3\sigma_T}{64\pi^2}\int dx\,dy\,dz\,dl\,\frac{\rho_L(x,y,z)n_e(l)}{s^4}[(y-p)^2 - x^2]\,, \quad (27)$$

where $P = \sqrt{Q^2 + U^2}$.

We assume a spatial luminosity density of the form

$$\rho_L(r) = \rho_L(0)(1 + r^2/r_c^2)^{\beta}\,, \quad (28)$$

where $\rho_L(0)$ is the central luminosity density and r_c is the core radius. As a specific example, we choose $\beta = -3/2$, which implies that the surface brightness scales like r^{-2} power law for large radii. Such a power law is commonly observed for giant elliptical and cD galaxies (Oemler & Tinsley 1979). The total luminosity is dictated by the outer cutoff, which we take to be $100r_c$. However, the scattering results we discuss are essentially independent of the cutoff because they depend upon integrals of functions which fall much more steeply with r than $\rho_L(r)$. We assume a radial distribution of the scattering medium given by

$$n_e(r) = n_c(1 + r^2/r_c^2)^{\gamma}\,. \quad (29)$$

We are primarily interested in the scattering in the halo; we include the core r_c to prevent an unrealistic divergence at the origin (as occurs in eq. [6]). As a specific example, we choose $\gamma = -\frac{1}{2}$, which is roughly appropriate when the scattering medium is part of a cooling flow (White & Sarazin 1987; Meiksin 1990), based on model fits to X-ray observations. There are complications in using these results to infer the scattering profile. In the models the X-ray intensity constrains $\langle n_e^2 \rangle$ but $\langle n_e \rangle$ can be varied by adjusting the gas clumping. Since the scattered intensity is proportional to $\langle n_e \rangle$, this yields a range in I, which Wise & Sarazin (1992) have shown for the

galaxy M87 can be as much as 40%. In addition, the loss of ionized gas by recombination and star formation alters the inferred scattering density.

Substituting equations (28) and (29) into equation (27) we find

$$[I] = \frac{3\sigma_T \rho_L(0) n_c r_c^2}{64\pi^2} \int \frac{d\tilde{x}\, d\tilde{y}\, d\tilde{z}\, d\tilde{l}}{\tilde{s}^4(1+\tilde{x}^2+\tilde{y}^2+\tilde{z}^2)^{\beta}(1+\tilde{l}^2+\tilde{\rho}^2)^{\gamma}} \times [\tilde{s}^2 + (\tilde{l}-\tilde{z})^2],$$

$$[P] = \frac{3\sigma_T \rho_L(0) n_c r_c^2}{64\pi^2} \int \frac{d\tilde{x}\, d\tilde{y}\, d\tilde{z}\, d\tilde{l}}{\tilde{s}^4(1+\tilde{x}^2+\tilde{y}^2+\tilde{z}^2)^{\beta}(1+\tilde{l}^2+\tilde{\rho}^2)^{\gamma}} \times [(\tilde{y}-\tilde{p})^2 - \tilde{x}^2], \quad (30)$$

where the dimensionless quantities $\tilde{x}$, $\tilde{y}$, $\tilde{z}$, $\tilde{l}$, $\tilde{s}$, and $\tilde{p}$ are x/r_c, y/r_c, etc., respectively. The integral has been evaluated using Romberg integration at 20 impact parameters.

The calculated polarization as a function of r, Π, is shown in Figure 5. Because of the four-dimensional nature of the integral, the numerical computation is quite time-consuming. Near the core radius, up to 10^{11} function evaluations per impact parameter were done. The relative accuracy was roughly a few percent in the inner regions. Note that $\Pi \to 0$ as $r \to 0$, since the source illuminates the line of sight symmetrically, and that $\Pi \to \frac{1}{2}$ as $r \to \infty$ (beyond the cutoff) when the point-source approximation is good. The figure shows that it is necessary to be many core radii ($r > 10r_c$) from the center before Π has risen to even one-half its asymptotic value. Figure 6 shows the ratio of I and P for the extended source to I and P for a point source. It can be seen that I and especially P are reduced significantly as the impact parameter approaches the core of the galaxy. Consequently, the intensity of polarized emission is much less than would be predicted given I and the asymptotic value of Π.

Since the quadratures are time-consuming, we give two empirical rules for the total and polarized intensity as a function of radius for extended sources:

$$I(r) \simeq I_{pt}(r) \frac{L_{cyl}(r) + L_{cyl}(r_c)}{L} \quad (31)$$

and

$$P(r) \simeq \frac{1}{2} I_{pt}(r) \frac{L_{sph}(r)}{L}. \quad (32)$$

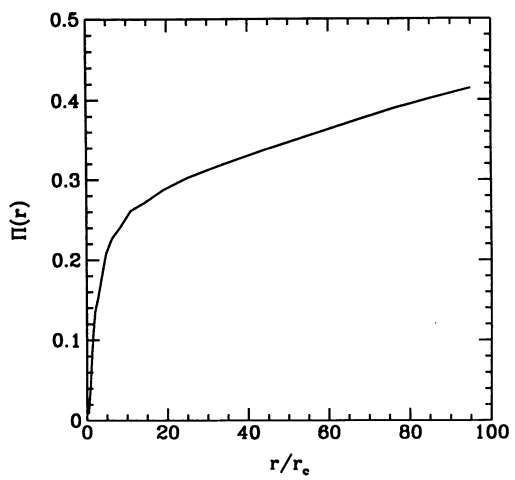

FIG. 5.—Polarization as a function of radius for an extended source given by eq. (30).

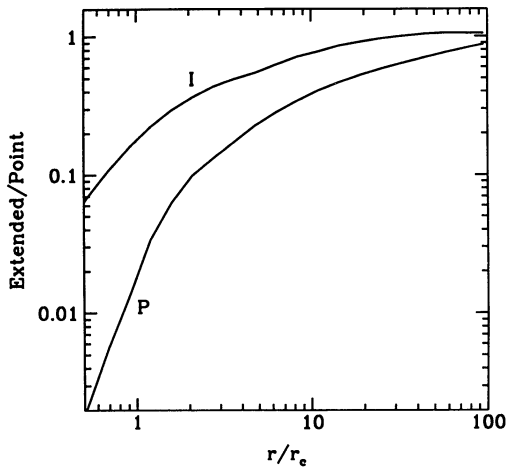

FIG. 6.—The ratios of the extended to point-source scattered intensities for I and P.

Here $L_{cyl}(r)$ and $L_{sph}(r)$ represent integrations of equation (28), giving the total luminosity within a cylinder and sphere of projected radius r, respectively. $I_{pt}(r)$ is the point source intensity (see eq. [7]) given by

$$I_{pt}(r) = \frac{L\sigma_T r_c n_c}{8\pi^2 r^2}. \quad (33)$$

Our rules of thumb given above are accurate to within 30% for $1 \le r/r_c \le 100$. Inside the core of the galaxy the values of I and P change too rapidly to be represented accurately by empirical laws. The total luminosity of the galaxy, idealized as a point source, provides a good fit only at large radii. For an extended source both the scattered intensity and polarized intensity are reduced by a significant fraction within about 10 core radii.

3.2. *cD Galaxies*

In this section we predict the intensity of scattered light from cD galaxies. Such galaxies have two desirable properties: (1) they are embedded in massive cooling flows, and (2) they are usually the most luminous galaxy in the cluster in which they reside. A luminous source in a dense scattering gas gives us the most favorable conditions for observing scattered light. We examine two galaxies in detail: M87 and NGC 1275. Each is associated with a cooling flow and each is the dominant galaxy in its cluster. We assume that the scattering gas is centered on the galaxy and that the galaxy acts as an extended source of luminosity. We make use of our results from § 3.1.

NGC 1275 has an enormous cooling flow, $\sim 300\ M_\odot\ \mathrm{yr}^{-1}$, and the total mass of gas lying within 200 kpc is estimated to be $10^{13}\ M_\odot$ (Fabian et al. 1981). We assume that the luminosity density and electron scattering gas are given by equations (28) and (29), respectively. We take $\beta = -3/2$ and $\gamma = -1/2$, as discussed in § 3.1. Integrating equation (29) and expressing n_c in terms of the total mass, M_{tot} within the radius r_g, we find

$$n_c = \frac{M_{tot}}{2\pi m_p r_c^2}\left(\frac{7}{8}\right)\left[\frac{r_g}{r_c}\sqrt{\frac{r_g^2}{r_c^2}+1} - \ln\left(\frac{r_g}{r_c} + \sqrt{\frac{r_g^2}{r_c^2}+1}\right)\right]^{-1}, \quad (34)$$

where m_p is the proton mass. The $(\frac{7}{8})$ that appears in equation (34) assumes that the gas is composed of 75% ionized hydrogen

and 25% doubly ionized helium by mass. The core radii for both scattering and luminosity densities are assumed to be 3.2 kpc, based on the V-band observations of Oemler (1976). We find $n_c \sim 0.45$ cm^{-3}. L_V is known from the absolute visual magnitude of -24.27 (Oemler 1976). Finally, we assume an outer cutoff in the luminosity density at $r_{\rm cut} = 100 r_c$ and solve for $\rho_{L_V}(0)$. By integrating equation (28), we find

$$\rho_{L_V}(0) = \frac{L_V}{4\pi r_c^3}\left[\ln\left(\frac{r_{\rm cut}}{r_c} + \sqrt{\frac{r_{\rm cut}^2}{r_c^2} + 1}\right) - \frac{(r_{\rm cut}/r_c)}{\sqrt{(r_{\rm cut}^2/r_c^2) + 1}}\right]^{-1} \quad (35)$$

and determine $\rho_{L_V}(0) = 2.96 \times 10^{-23}$ ergs s^{-1} cm^{-3}. Knowing $\rho_{L_V}(0)$ and n_c, it is now possible to calculate the total and polarized intensities for our model galaxy from equation (30).

Figure 7*a* shows the total and polarized intensities, along with 1% of the background intensity in V. The background is composed of galaxy plus sky emission and is a function of r. We include it as an effective lower bound that the total and polarized intensities must exceed for any hope of detection. As a practical matter, current instruments can measure an intensity $\geq 1\%$ of the background (Miller & Goodrich 1988). We take the sky intensity in V to be 21.9 mag arcsec^{-2} (Pilachowski et al. 1989). The contribution of the galaxy to the background decreases at shorter optical wavelengths, but the intensity of the scattered light is similarly diminished. As we will show in § 3.3, when the scattered light derives from a bluer source (such as an AGN) it is advantageous to observe in U or B. In this example, however, little can be gained by doing so. An additional difficulty in making measurements of polarization fractions below 1% of the galaxy emission is the grain-induced polarization that affects light traveling through the interstellar medium of the Galaxy. Studying a large sample of nearby stars, Serkowski, Mathewson, & Ford (1975) found an empirical expression for the maximum polarization, $\Pi \leq 0.09\, E(B-V)$, where $E(B-V)$ is the differential extinction. For $|b| \leq 20°$ the range of $E(B-V)$ is roughly 0.01 to 0.1 (Burstein & Heiles 1982), with the lowest values found toward the poles. Hence, the grain-induced polarization should be less than 1% of the emission of the galaxy. Our results show that detecting the scattered light in NGC 1275 is currently impossible at optical wavelengths. At no point is I above the 1% background level. Furthermore, the polarized intensity is a very small fraction of the total scattered intensity. The maximum of polarized emission occurs just beyond the core radius, only 27.8 mag arcsec^{-2}, or roughly 3 mag fainter than the 1% level of the background.

We include a second example with a different core radius and scattering gas density to suggest that it will generally be impossible to observe scattered light in the vicinity of a cD galaxy. This example, M87, has a maximum mass inflow rate of 40 $M_\odot$ yr^{-1}. Here n_c is based on the cooling flow model fit to *Einstein* X-ray data (White & Sarazin 1988). Oemler (1976) gives the core radius of 2.2 kpc, and we match the number density of the cooling flow model there. The result is $n_c = 0.75$ cm^{-3}. The luminosity density is calculated in the same manner as above, using equation (35), for an absolute visual magnitude of -23.53 (Oemler 1976). We find $\rho_{L_V}(0) = 4.6 \times 10^{-23}$ ergs s^{-1} cm^{-3}.

Figure 7*b* shows the values of 1% of the galaxy plus sky intensity, I, and P for M87. Again, the scattered and polarized intensities lie below the 1% level. *We conclude that the intensity of visible scattered light from a cD galaxy immersed in a cooling flow is too small to be observed.*

3.3. *A cD Galaxy with an Isotropic Active Nucleus*

In this section we add an active nucleus to the cD galaxy. In our model we assume (1) that the luminosity of the central nucleus is equal to that of the surrounding galaxy in V; (2) that the emitted light from the nucleus is isotropic; (3) that the nucleus is a point source; (4) that the nuclear luminosity is constant; and (5) that the emission is unpolarized. In the next section we consider an anisotropic flux from the central source. For relaxation of some of these restrictions we refer the reader to Wise & Sarazin (1992) and Sarazin & Wise (1993).

In this section we will compare the scattering in U, B, and V

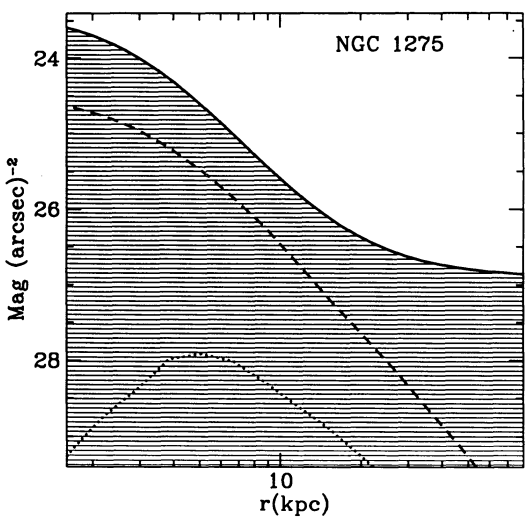

FIG. 7*a*

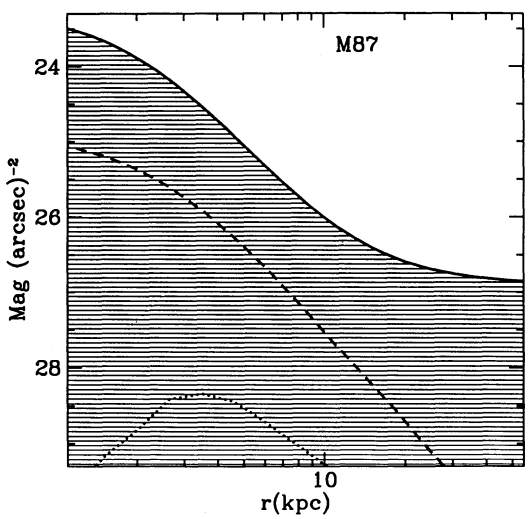

FIG. 7*b*

FIG. 7.—(*a*) Scattered brightness profile of NGC 1275 (I and P) is compared to the threshold for detection, which is 1% of the sum of the extended diffuse galactic emission and the sky. I, P, and the 1% background level are represented by the dashed, dotted, and solid lines, respectively. At no point is the scattering detectable in optical wavelengths with current instruments (see § 3.2). (*b*) Same as Fig. 7*a* for M87.

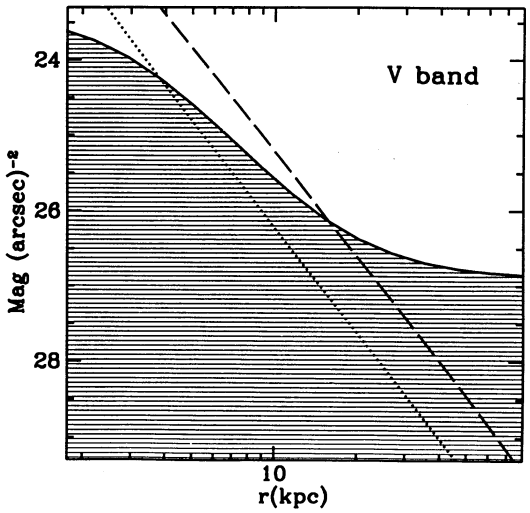

FIG. 8*a*

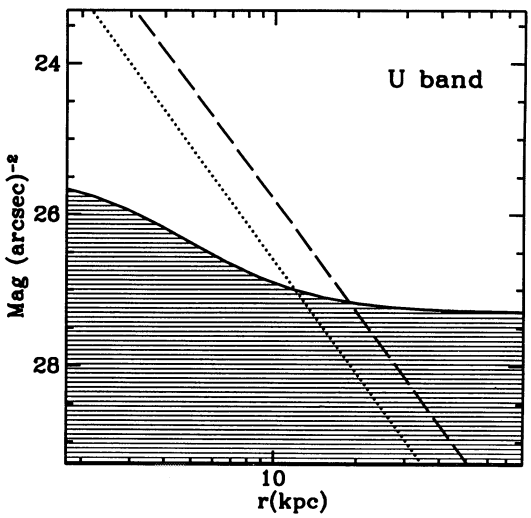

FIG. 8*c*

FIG. 8.—Same as Fig. 7*a* except that a central point source of luminosity $L_\nu = 1.54 \times 10^{45}$ ergs s^{-1} (equal to that of the background galaxy) is included in the calculation for three wavelength bands, *U*, *B*, and *V*. *I*, *P*, and the 1% background level are represented by the dashed, dotted, and solid lines, respectively. Note that *I* and *P* exceed the detection threshold for this case.

bands. Thus, we assume (6) that the parent galaxy has a spectrum of the form

$$F_\nu^{\rm gal} \propto \begin{cases} \nu^{-2.1}, & \text{for } \nu < 10^{14.83} \text{ Hz}, \\ \nu^{-6.0}, & \text{for } \nu > 10^{14.83} \text{ Hz}, \end{cases}$$

and the active nucleus of the form

$$F_\nu^{\rm agn} \propto \begin{cases} \nu^{-1}, & \text{for } \nu < 10^{14.85} \text{ Hz}, \\ \nu^{0}, & \text{for } \nu > 10^{14.85} \text{ Hz}. \end{cases}$$

These spectral distributions are rough fits to the "standard galaxy" taken from Malkan & Oke (1983) and to AGNs taken from Francis (1993). The *U*, *B*, and *V* intensities are determined by integrating the above distributions over the appropriate frequency ranges.

We choose the same parameters as those for NGC 1275 except that we include a central point source of equal luminosity, $L_\nu^{\rm agn} = 1.54 \times 10^{45}$ ergs s^{-1} at the center. Far outside the core of the electron scattering distribution, equation (7) implies that the scattered intensity from the active nucleus goes as $1/r^2$. Figures 8*a*–8*c* show the total and polarized intensities for *V*, *B*, and *U*. For *U* and *B* we take the sky intensity to be 22.2 and 23.0 mag arcsec^{-2}, respectively (Neizvestnyi 1982; Pilachowski et al. 1989). In *V* the total and polarized intensities exceed the 1% background level for radii less than 15 kpc and 4 kpc, respectively. Moving to *U*, these radii become 19 kpc and 13 kpc, respectively. Within 10 kpc the measured polarization, *P*, exceeds several percent in *U*. This change is largely due to the decreased galaxy background.

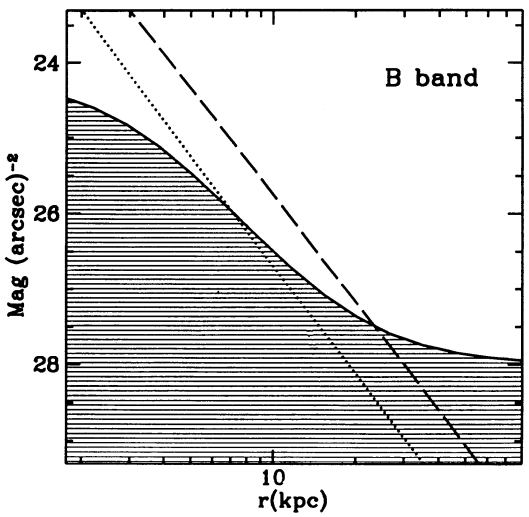

FIG. 8*b*

For all three bands, the detectable effect is due completely to the presence of the active nucleus. Obviously, if the nucleus were brighter than the value we assigned it, the values of *I* and *P* would be proportionally larger. Active galaxies can have luminosities up to and exceeding 10^{47} ergs s^{-1} (Weedman 1986), roughly 100 times the luminosity of the most luminous cD galaxy. At a luminosity of 10^{47} ergs s^{-1} the scattered *I* and *P*, for parameters similar to NGC 1275, could be detected out to roughly 200 kpc. Although a correlation exists between the luminosities of the active nucleus and the parent galaxy, we note that we have already adopted a near-maximum estimate for the luminosity of the cD (Hutchings et al. 1984) whose background serves to obscure the scattered light. Many more galaxies may be visible in scattered light; this depends upon how many have nuclei that outshine the rest of the galaxy and, at the same time, have sufficiently high Thomson optical depths.

3.4. *Active Nucleus with Beamed Radiation*

There have been recent suggestions that the brightest AGNs are those that are being beamed toward us (Barthel 1989), though there is some evidence against this suggestion (Boroson 1992). With this in mind, we now investigate a model that has its radiation beamed at an angle ϕ relative to the line of sight of the observer. Let L_b be the apparent luminosity for an observer when the beam is aligned with the line of sight. Relative to the isotropic case, with $L = L_b$, the intensity of scattered light will be diminished since the emissivity is confined to the cone of radiation. From equations (4) approximate expressions for the

intensity of scattered and polarized light are

$$I \simeq \frac{I_0}{p^2} \Delta\theta \sin \phi(1 + \cos^2 \phi) , \quad (36)$$

and

$$P \simeq \frac{I_0}{p^2} \Delta\theta \sin \phi(1 - \cos^2 \phi) \quad (37)$$

Here p is the impact parameter, $\Delta\theta$ is the angular width of the beam, and $I_0 = 3L_b n_c \sigma_T r_c/64\pi^2$. These formulae are accurate when the beam is not pointed near the line of sight and $\Delta\theta$ is small. As an example, assume the gas distribution of NGC 1275, $L_b = 10^{47}$ ergs s^{-1} and $\Delta\theta = 15°$. If the beam is perpendicular to the line of sight, $I \simeq 9.0 \times 10^{-13}/p^2$ (kpc) ergs s^{-1} cm^{-2} arcsec^{-2} or $18.4 + 5 \log_{10}[p(\text{kpc})]$ mag arcsec^{-2} and $\Pi = 1.0$. Thus the scattered radiation from the beam could be observed out to $\sim$80 kpc before it drops below the 1% background level. Even if the beam is not pointed toward us, its scattered light may be visible and may be used to determine the orientation of the beam (Fabian 1989; Wise & Sarazin 1992).

3.5. *Spectral Lines*

The presence of strong spectral lines from an AGN provides another possible strategy for detecting scattered light. If the brightness of the emission line from the AGN is significantly larger than the brightness of the continuum of the AGN plus galaxy background, then it may be advantageous to use a filter narrower than the U, B, or V-band centered on the line frequency to enhance the signal-to-noise ratio of an observation. Scattered light from regions far from the nucleus could be more easily seen because background contamination would be reduced.

There are several complications. First, the scattered line spreads in frequency because the photons scatter off a hot gas (see § 2.1). The expected temperatures in cooling flows range from 10^6 K (inner few kiloparsecs) to 10^8 (outermost regions) (Fabian et al. 1991), so that a scattered optical line with a wavelength of $\sim$5000 Å will be smeared from 60 Å to 600 Å. If the nuclear continuum is flat over similar bandwidths, the smearing reduces the brightness ratio of the nuclear emission line to the nuclear continuum.

Observations of AGNs show that the strongest lines are roughly 3 times the AGN continuum. Many of these lines, such as Hα, have velocity widths of a few thousand kilometers per second or about a few hundred angstroms (Osterbrock & Mathews 1986). Narrower lines such as [O III] are less useful: their maximum intensity per frequency interval is comparable to Hα, but the smearing will reduce their intensities relative to the continuum by a much larger factor.

To make an estimate we proceed as follows. Some emission lines, such as Hα, arise almost solely from the photoionization of clouds in the inner 100 pc of the nucleus. In § 3.3 we have shown that the most promising region for detecting scattered light is within the inner 20 kpc of the nucleus. At these radii the gas temperature will be $\sim 10^6$ K and Hα will be smeared $\sim$100 Å. Since the smearing is less than the intrinsic line width, the ratio of scattered line to scattered nuclear continuum will be roughly 3. If the background from the galaxy is roughly flat over the same bandwidth, then the filtered intensity may be enhanced by up to a factor of 3, compared to the broad-band case. Thus, strong emission lines emanating from an AGN could be marginally helpful for observing scattered light in regions of a cooling flow outside of the nucleus.

One complication is that many cooling flows exhibit the same optical emission lines as found in AGNs (Stockton & MacKenty 1987). In this case, the galactic background includes a component that is not reduced by using a filter, and the usefulness of the emission lines is decreased. Still, one could distinguish the origin of this emission by polarization measurements and possibly by subtracting the narrower background emission line of the cooling flow.

3.6. *Off-Center Gas Distribution*

We have shown that scattered and/or polarized light can currently be detected in a cD galaxy with an active nucleus of luminosity roughly equal to or greater than that of the rest of the galaxy. In this section we use the results from § 2.4 to examine the situation when part of the scattering gas is not centered on the cD galaxy. For a galaxy of fixed luminosity, a scattering halo typical of a cD galaxy ($\alpha = 1$), and a clump of fixed column density, we showed that the ratio of the clump scattered brightness to that of the halo increases with distance from the galaxy center. Two additional factors must be taken into account to assess the visibility of scattering from such off-center clumps: (1) the diffuse background of the galaxy and (2) the intrinsic sky level.

A possible example of an off-center density distribution is the radio source PKS 0745−191 (Fabian et al. 1985). This galaxy is immersed in a hot gas that is cooling at a rate of up to 1000 $M_\odot$ yr^{-1}. The X-ray image of this source extends to roughly 200 kpc, with a peak of emission that lies 30 kpc from the center of the galaxy (indicating a possible density maxima). From the optical observations of Fabian et al. (1985) we arrive at the following values for the galaxy: $r_c^{\text{gal}} = 9$ kpc, $r_{\text{cut}} = 45$ kpc, $m_V = 16$, and $L_V = 1.09 \times 10^{45}$ ergs s^{-1}. The cutoff radius of the galaxy is uncertain but its actual value does not change our results significantly. From X-ray data, the average density within 30 kpc of the intensity peak is 0.06 cm^{-3} (Fabian et al. 1985). We take the scaling radius of the off-center density peak to be equivalent to the core radius of the cD galaxy, $r_c^{\text{cl}} = 9$ kpc. Then, assuming for the scattering gas a power law identical to equation (6) where $\alpha = 1$, we arrive at $n_c^{\text{cl}} = 0.13$ cm^{-3}. The luminosity is assumed to be emanating from a AGN for the purpose of calculating the scattering. (Consulting Fig. 6, we expect the errors in the total scattered intensity to be less than a factor of 2). For the purpose of determining the background emission, we assume that the galaxy's luminosity density is extended, following equation (28) where $\beta = -3/2$.

Using the information from the previous paragraph, we now estimate the intensity at a distance r_c^{cl} from the scattering gas center. We will assume that the center is coplanar with the galaxy center and the clump gas has $\alpha = 1$. We find the intensity of the polarized emission, P, to be 27.5 mag arcsec^{-2}, about 1 mag brighter than the examples in § 3.2 at the equivalent radius. In our power-law model the intensity diverges as the density singularity is approached (see § 2.4); the actual maximum is dictated by the core radius of the clump, which, of course, is unknown. Overall, there is a region roughly 10 kpc in diameter near the density peak with I and P above the 1% background level. Thus, we can only conclude that if the core radius $\lesssim$10 kpc, scattering may be visible. If the gas center lies out of the plane of the galaxy, then the polarized intensity will be reduced significantly relative to a gas center in the plane. Thus, it may be possible to detect relatively dense regions of

hot gas residing near a luminous galaxy. If detected, it may be possible to determine the position along the line of sight from the fractional polarization.

Finally, we point out that the presence of an active nucleus with a luminosity greater than that assumed above lifts the level of scattered light proportionally. Scattering may be used to probe the galaxy's gas and cooling flow and thus represents a potentially complementary source of information to that provided by X-ray observations. In a cooling flow, for example, one would like to know where the infalling gas is converted into stars plus the length scale and growth rate of thermal instability. These angular scales are typically smaller than the resolution of X-ray telescopes but easily within the range of optical instruments.

4. CONCLUSIONS

In this paper we have outlined the nature of scattering in a hot gas surrounding a luminous galaxy or an AGN for a variety of simple models. We began by considering a point-line luminosity source embedded in scale-free electron power laws. We derived asymptotic estimates for the scattering intensity and polarization fraction in the neighborhood of the density peak and the luminosity source. We complemented these analytic results with numerical calculations of the scattering intensity, polarization fraction, and angle of polarization for single and multiple point-like luminosity sources. The large-scale patterns illustrate the effects of interference between sources. For an extended luminosity source we showed that the interference decreased the polarization fraction in the vicinity of the source.

We applied our results to investigate several potential types of scattering in the vicinity of galaxies. For a typical cD galaxy (without an active nuclei) the scattered galactic emission is too weak to be detected with current instruments at optical wavelengths. However, those galaxies with an active nucleus and/or off-center gas are possibilities.

An active nucleus increases the flux of scattered radiation and is so small that interference effects are negligible. We show that when a galaxy has an active nucleus equal in luminosity to the parent galaxy, the total polarized and scattered intensities in the inner 5–30 kpc exceed the 1% background level. This is a conservative estimate, since the luminosity of many nuclei exceed their parent galaxies by factors of 10 to 100; for these more luminous examples the total polarized and scattered light becomes visible on much larger size scales. For typical galaxy and AGN spectra, it is significantly easier to measure the scattering at short wavelengths (i.e., U). If an active galaxy has an obscuring dust torus or is beaming its radiation in a direction away from the line of sight, it may be possible to determine the orientation of the torus/beam by searching for the cone of scattered light. There is only modest advantage to using a narrow-band filter centered on an emission line, because the typical continuum associated with the active nucleus is only a factor of 3 less in intensity than the scatter-broadened emission lines.

For galaxies with off-center gas distributions, detection is easier because of the reduced background from the galaxy at the gas center and a high degree of polarization. The polarization fraction reaches a local maximum as the impact parameter approaches the off-center distribution. In our example, PKS 0745−191, the scattered and polarized intensity were greater than 1% of the background intensity of the galaxy and sky for a region roughly 10 kpc in diameter. When an active nucleus is present, both the intensity of the scattered radiation and the size of the region grow. Hence, clumps of ionized gas in the environment surrounding the galaxy should be detectable by searching for regions of polarized emission.

We conclude that there are a number of promising observational possibilities offered by polarized scattering that occurs near galaxies, especially those with AGN's.

This research was supported in part by grants NSF-AST-8657467, NSF-AST-8913112, NSF-AST-9119475, NAGW-2224. We thank G. Djorgovski, R. Goodrich, J. Krolik, C. Sarazin, I. Wasserman, and the referee for useful comments.

REFERENCES

Barthel, P. D. 1989, ApJ, 336, 606
Boroson, T. A. 1992, ApJ, 399, L15
Burstein, D., & Heiles, C. 1982, AJ, 87, 1167
Canizares, C. R., Stewart, G. C., & Fabian, A. C. 1983, ApJ, 272, 449
Chambers, K. C., Miley, G. K., & van Breugel, W. 1987, Nature, 329, 604
Cowie, L. L., Hu, E. M., Jenkins, E. B., & York, D. G. 1983, ApJ, 272, 29
Crawford, C. S., & Fabian, A. C. 1989, MNRAS, 239, 219
di Serego Alighieri, S., Cimatti, A., & Fosbury, R. A. E. 1992, Arcetric Astrophysics preprint No. 17
Djorgovski, S., Spinrad, H., Pedelty, J., Rudnick, L., & Stockton, A. 1987, AJ, 93, 1307
Fabian, A. C. 1989, MNRAS, 238, 41p
Fabian, A. C., et al. 1985, MNRAS, 216, 923
Fabian, A. C., Hu, E. M., Cowie, L. L., & Grindlay, J. 1981, ApJ, 248, 47
Fabian, A. C., Nulsen, P. E., & Canizares, C. R. 1991, Astron. Astrophys. Rev., 2, 191
Francis, P. J. 1993, ApJ, 407, 519
Gil'fanov, M. R., Syunyaev, R. A., & Churazov, E. M. 1987, Soviet Astron. Lett., 13, 3
Gradshteyn, I. S., & Ryzhik, I. M. 1980, Table of Integrals, Series, and Products (New York: Academic Press)
Heckman, T. M. 1981, ApJ, 250, L59
Hutchings, J. B., Crampton, D., & Campbell, B. 1984, ApJ, 280, 41
Jones, C., & Forman, W. 1984, ApJ, 276, 38
Kent, S. M., & Sargent, W. L. W. 1979, ApJ, 230, 667
Malkan, M. A., & Oke, J. B. 1983, ApJ, 265, 92
McNamara, B. R., & O'Connell, R. W. 1993, AJ, 105, 417
Meiksin, A. 1990, The Edwin Hubble Centennial Symposium (A.S.P. Conference Series) (San Francisco: ASP), 50
Miller, J. S., & Goodrich, R. W. 1988, Nature, 331, 685
Neizvestnyi, S. I. 1982, Bull. Special Astrophys. Obs., 16, 41
Oemler, A. J. 1976, ApJ, 209, 693
Oemler, A. J., & Tinsley, B. M. 1979, AJ, 84, 985
Osterbrock, D. E., & Mathews, W. G. 1986, ARA&A, 24, 171
Pilachowski, C. A., Africano, J. L., Goodrich, B. D., & Binkert, W. S. 1989, PASP, 101, 707
Rybicki, G. B., & Lightman, A. P. 1979, Radiative Processes in Astrophysics (New York: Wiley)
Sarazin, C. L. 1986, Rev. Mod. Phys., 58, 1
Sarazin, C. L., O'Connell, R. W., & McNamara, B. R. 1992, ApJ, 397, L31
Sarazin, C. L., & Wise, M. W. 1993, ApJ, 411, 55
Serkowski, K., Mathewson, D. S., & Ford, V. L. 1975, ApJ, 196, 261
Stewart, G. C., Canizares, C. R., Fabian, A. C., & Nulsen, P. E. J. 1984a, ApJ, 278, 536
Stewart, G. C., Fabian, A. C., Jones, C., & Forman, W. 1984b, ApJ, 285, 1
Stockton, A., & MacKenty, J. W. 1987, ApJ, 316, 584
Syunyaev, R. A. 1982, Soviet Astron. Lett., 8, 175
Weedman, D. W. 1986, Quasar Astronomy (Cambridge: Cambridge Univ. Press)
White, R. E., III, & Sarazin, C. L. 1987, ApJ, 318, 612
———. 1988, ApJ, 335, 688
Wise, M. W., & Sarazin, C. L. 1990, ApJ, 363, 344
———. 1992, ApJ, 395, 387